ACS OMEGA

Open Access

http://pubs.acs.org/journal/acsodf

Article

Promoting the Calcified Roasting of Vanadium Slag Based on the CeO_2-Catalytic Oxidation Mechanism

Zongyuan Xu,[§] Kang Tang,[§] Yan Chen, Qian Zhang, Jun Du,* Zuohua Liu, and Changyuan Tao*

Cite This: *ACS Omega* 2024, 9, 16810−16819

Read Online

ACCESS | Metrics & More | Article Recommendations

ABSTRACT: Calcification roasting−acid leaching is a clean, efficient, and environmentally friendly process, but in the roasting process, the local temperature is often too high, the heat release is not timely, and the heat transfer is blocked. Furthermore, the material is easy to sinter, which affects the final vanadium extraction effect. In this paper, a small amount of CeO_2 was introduced in the roasting process of vanadium slag to promote the calcified roasting. The results showed that the vanadium leaching rate reached 93.17% with the addition of 0.1 wt % CeO_2 at a roasting temperature of 750 °C, which was higher than that obtained without CeO_2 addition (90.00%). The results of XPS, XRD, and SEM-EDS analyses confirmed that adding CeO_2 to the roasted clinker significantly increased the proportion of pentavalent vanadium to the total vanadium by up to 28.64%. O_2-TPD analysis revealed an enhanced chemisorbed oxygen with the CeO_2-assisted roasting, indicated the activation of oxygen by CeO_2, and resulted in an enhanced oxidation of vanadium. The work in this paper establishes an alternative route for catalytic oxidation-enhanced vanadium slag roasting, which can improve the utilization of vanadium slag at relatively lower temperatures under the action of CeO_2 and is of positive significance in solving the problems of sintering and energy consumption in the roasting process.

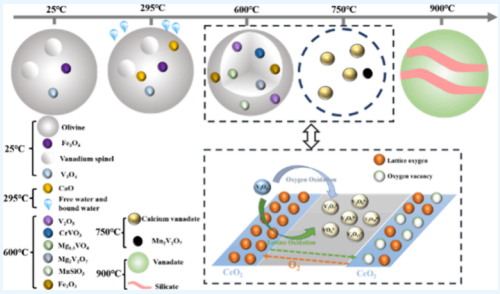

1. INTRODUCTION

Vanadium is ranked 22nd in terms of earth abundance between 0.02 and 0.03%.[1] Vanadium is widely used in batteries, aerospace, iron and steel smelting, petroleum, catalyst, and other fields[2,3] because of its excellent physical and chemical properties such as high tensile strength, high hardness, and corrosion resistance.[4] At present, vanadium−titanium−magnetite is the main vanadium extraction raw material,[5,6] which produces vanadium-containing hot metal in the process of steelmaking and then oxidizes and blows to get converter vanadium slag.[6,7] Part of the vanadium spinel phase in vanadium slag is wrapped by a silicate phase, resulting in a large amount of vanadium that cannot be effectively leached.[8,9] Roasting plays a very important role in the vanadium extraction process. One of the most traditional roasting methods is sodium roasting; that is, sodium salts (NaCl, $NaCO_3$, etc.) are added as additives during the roasting process, and the vanadium spinel phase is oxidized to sodium vanadate that is easily soluble in water. However, the roasting will produce Cl_2, HCl, SO_3, SO_2, and other corrosive gases harmful to the environment.[3,10,11] With the improvement of public awareness of environmental protection, the calcified roasting vanadium extraction method has attracted more and more attention because of its environmental friendliness and clean and efficient advantages. In this method, calcium compounds (CaO, $CaCO_3$, etc.) are added to the roasting process. Vanadium in vanadium slag reacts with calcification additives to form acid-soluble calcium vanadate to improve the leaching rate of vanadium.[6,12]

In recent years, research related to strengthening roasting has been reported, such as the proposed $BaCO_3$/CaO composite roasting,[13] MgO/CaO composite roasting,[9] manganese roasting,[14] microwave roasting,[15] and so forth. It is mostly understood and emphasizes the role of roasting vanadium slag from the destruction of the spinel phase structure. For the roasting process of vanadium slag, the essence is to realize the valence state change of the vanadium element through electron transfer to convert vanadium into soluble pentavalent vanadate. However, there is still a lack of sufficient experimental analysis and theoretical research to further understand the initial oxygen activation and electron-transfer mechanism. Song et al.[16] reported that the synergistic effect between CeO_2 and MnO_x could provide more amounts of oxygen vacancy, the highest concentration of Mn^{3+}, and the highest Ce^{3+} contents, which resulted in an outstanding oxygen mobility, causing the improvement of catalytic activity. Li et

Received: February 6, 2024
Revised: March 15, 2024
Accepted: March 19, 2024
Published: March 28, 2024

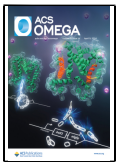

Table 1. Components of Vanadium Slag (wt %)

component	O	Fe	V	Ti	Si	Mn	Ca	Cr	Mg	others
amount	34.94	34.45	8.70	5.82	4.32	6.89	1.43	1.29	0.87	1.29

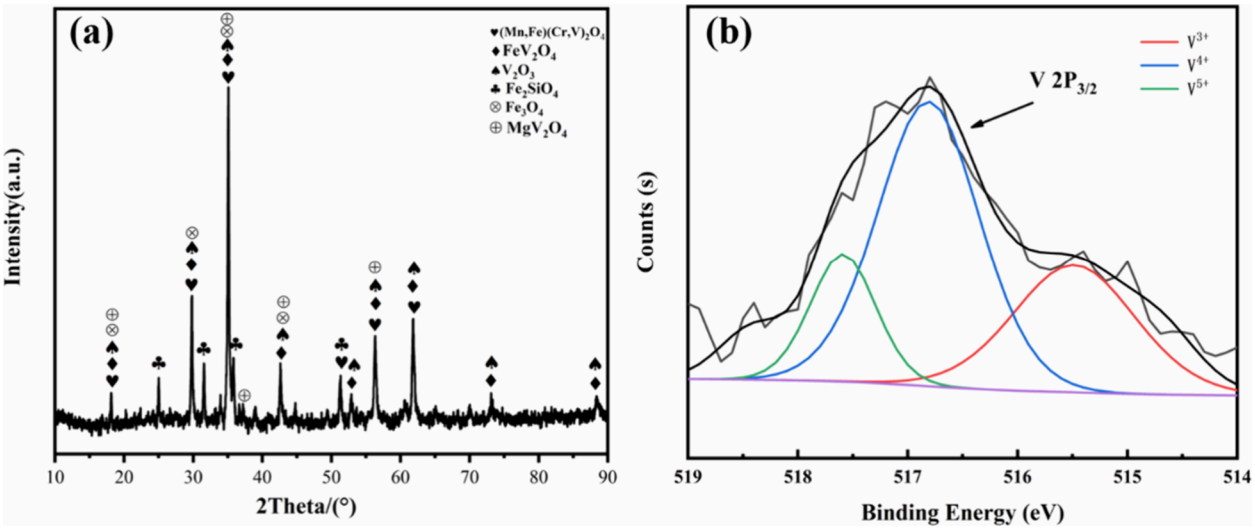

Figure 1. (a) XRD pattern and (b) XPS pattern of vanadium slag.

al.[17] reported that cerium dioxide nanoparticles have the most active surface oxygen vacancies that determine the catalytic activity and have the strongest activation capacity, contributing to high reactivity under extremely inert conditions. The roasting process of vanadium slag is a typical oxidation process, and the activation of molecular oxygen has emerged to be an important step. CeO_2 has been widely used in the field of catalysts due to its excellent redox properties and inherent structural defects.[18] The two oxidation states of Ce^{3+} and Ce^{4+} can achieve rapid and reversible conversion according to the content of oxygen in the external environment.[19] Therefore, oxygen vacancy defects easily appear in the lattice of CeO_2. These characteristics not only make CeO_2 have excellent oxygen release ability but also make oxygen vacancies diffuse rapidly at high temperatures.

This paper introduces trace and cheap CeO_2 as a catalyst in the roasting process of vanadium slag to promote the activation of oxygen, thereby strengthening the calcification of the roasting of vanadium slag. In the presence of CeO_2, vanadium in the vanadium slag will be oxidized at an enhanced reaction rate. The introduction of CeO_2 as a catalyst in the calcification roasting process of the converter vanadium slag is expected to promote the conversion of vanadium from a low valence state to a high valence state and accelerate the destruction of the vanadium spinel phase to achieve an efficient recovery of vanadium at a lower temperature.

2. MATERIALS AND METHODS

2.1. Materials. The vanadium slag used in this paper was supplied by Panzhihua Iron and Steel Group (Sichuan Province, China) and was characterized after drying and sieving through a 200 mesh sieve. The composition and content of the main elements are shown in Table 1, and the phase composition by X-ray diffraction (XRD) is shown in Figure 1a. The vanadium slag is mainly composed of the spinel phase of FeV_2O_4, $(Mn, Fe)(Cr, V)_2O_4$, MgV_2O_4, and so forth, olivine phase such as Fe_2SiO_4, and free oxide phase such as V_2O_3, Fe_3O_4, and so forth. The valence state of V in the vanadium slag was analyzed by X-ray photoelectron spectroscopy (XPS), and the results are shown in Figure 1b. The proportions of V(III) (binding energy of $2p_{3/2}$ is 515.49 eV), V(IV) (binding energy of $2p_{3/2}$ is 516.81 eV), and V(V) (binding energy of $2p_{3/2}$ is 517.59 eV) are 29.32, 54.93, and 15.75%, respectively, among which the content of V(V) is the lowest. The roasting additives (calcium oxide and cerium dioxide) used in the experiment are analytical-grade reagents (AR, Cologne Chemical, China).

2.2. Experimental Procedure. The converter vanadium slag, calcium oxide, and cerium oxide were added to an agate mortar and mixed and ground for 20 min, then transferred to a 100 mL crucible, and roasted in a muffle furnace (SANTE STM-12-14Q, China). In the roasting process, the samples were investigated at different roasting temperatures, roasting times, and additive ratios. After roasting, the leaching experiments were carried out under the conditions of leaching temperature of 80 °C, 2 mol·L^{-1} sulfuric acid solution, liquid−solid ratio of 4:1 mL/g, leaching time of 30 min, and rotation speed of 400 rpm. After leaching, the concentration of vanadium in the filtrate was determined by an inductively coupled plasma emission spectrometer (ICP). The leaching efficiency was calculated using eq 1:[11]

$$\eta = \frac{V_L \times C_V}{m \times \omega} \times 100\% \quad (1)$$

where V_L (L) is the volume of leached liquid after filtration; C_V (g/L) is the concentration of vanadium in the leaching solution after filtration; m (g) is the mass of vanadium slag added to this experiment; and ω (wt %) is the mass fraction of vanadium in the slag.

2.3. Analytical Methods. The mineral composition of vanadium slag and roasted clinker was characterized by using an X-ray powder diffractometer (XRD, D/MAX-2500, Rigaku, Japan). The chemical composition of vanadium slag was analyzed by an X-ray fluorescence spectrometer (XRF, ARL

https://doi.org/10.1021/acsomega.4c01211
ACS Omega 2024, 9, 16810−16819

Perform'X, Thermo Fisher Scientific CDLtd, Switzerland). The morphology and element distribution of vanadium slag and roasted clinker were analyzed by scanning electron microscopy (SEM, Ultra Plus, Carl Zeiss, Germany) and X-ray energy dispersion spectroscopy (EDS, Oxford X-MAX, Carl Zeiss, Germany). Thermogravimetric (TG) and differential scanning calorimetry (DSC) analyses were performed using a synchronous thermal analyzer (TG-DSC, TGA/DSC1/1600LF, Mettler Corporation, Switzerland). The changes in the valence states of V and Fe during roasting were analyzed by X-ray photoelectron spectroscopy (XPS, Escalab-250Xi, ThermoFisher Corporation, Britain). The content of the V element in the leaching solution of calcined clinker was determined by an inductively coupled plasma emission spectrometry system (ICP-OES, ICAP6300, ThermoFisher Scientific, Britain). The oxygen adsorption capacity of the vanadium slag mixture was analyzed by an automatic chemisorbent analyzer (TPD, Belcat II, MicrotracBEL, Japan).

3. RESULTS AND DISCUSSION

3.1. Enhanced O_2 Chemisorption in the CeO_2−CaO Roasting Vanadium Slag. The O_2 adsorption capacity of the vanadium slag mixtures after the addition of CeO_2 was investigated by the O_2-TPD (temperature-programmed desorption) method. The experimental procedure was as follows: CaO−vanadium slag ($n(CaO)/n(V_2O_5)$ = 1) and CaO−CeO_2−vanadium slag ($n(CaO)/n(V_2O_5)$ = 1, $m(CeO_2)/m$(vanadium slag) = 1/1000) were heated from room temperature to 300 °C in an inert atmosphere at a rate of 10 °C per minute and purged for 60 min. After 30 min at a constant temperature, the temperature was lowered to 50 °C, and oxygen was introduced and purged with helium. The temperature was allowed to drop to room temperature, and then the temperature was increased to 1000 °C at 5 °C/min. Further, the O_2-TPD curves are shown in Figure 2. Both mixtures have three desorption peaks, and their peak locations are consistent. However, in the range 500−700 °C, the areas of both desorption peaks (18,336 and 8004) with the addition of CeO_2 were larger than those (14,268 and 6688) without the addition of CeO_2. This indicates that the addition of CeO_2 increased the amount of chemisorbed O_2 compared to that without CeO_2. Therefore, the mixture of vanadium slag-CaO−CeO_2 possesses more oxygen vacancies, and the higher O_2 adsorption predicted an enhanced O_2 activation ability and subsequently the increased amount of active oxygen species.

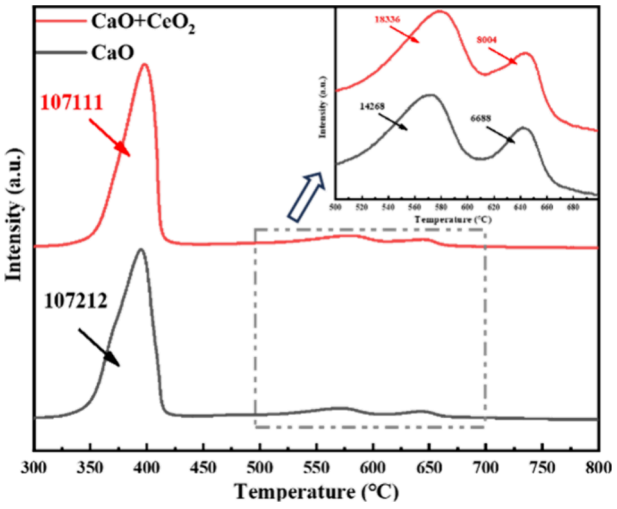

Figure 2. O_2-TPD diagram of the mixture of different additives and vanadium slag.

3.2. Thermolysis of CeO_2-Catalyzed Calcification of Vanadium Slag. In order to investigate the thermodynamic behavior of the calcification and CeO_2-catalyzed calcification roasting process, 10 g of vanadium slag was mixed homogeneously with CaO ($n(CaO)/n(V_2O_5)$ = 1) and CaO−CeO_2 ($n(CaO)/n(V_2O_5)$ = 1, $m(CeO_2)/m$(vanadium slag) = 1/1000), respectively. The two mixtures were subjected to TG-DSC measurements from room temperature to 1000 °C at a rate of 10 °C/min (Figure 3). The trends of the TG-DSC curves of the two mixtures are similar, but the weight increase is greater in the presence of CeO_2. Changes in the mass of the vanadium slag and the appearance of exothermic and absorptive peaks were observed at different temperature sections. The TG curve presented a mass increment beginning at 295 °C, indicating the oxidation by absorption of oxygen accompanied by an exothermic effect. There was a steep mass increment between 700 and 900 °C, and it is assumed that a large number of oxidation reactions took place. Therefore, the roasting temperatures at 295, 400, 430, 600, 700, and 900 °C are selected for the study in this paper. Furthermore, to investigate the generation of the vanadate phase at 700−900 °C, the roasting temperatures of 750, 800, and 850 °C were used in this study.

3.3. Effect of Roasting Temperature on Vanadium Slag. Vanadium slag was mixed with a certain amount of CaO and CeO_2 ($n(CaO)/n(V_2O_5)$ = 1, $m(CeO_2)/m$(vanadium slag) = 1/1000); a control group was set up at the same time ($n(CaO)/n(V_2O_5)$ = 1) for roasting at different temperatures for 2 h; and the vanadium leaching rate was determined after the leaching of roasted materials (leaching conditions: T = 80 °C, t = 30 min, 2 mol·L^{-1} sulfuric acid solution, and liquid−solid ratio 4:1 mL/g). The results of the experiments are shown in Figure 4.

The vanadium leaching rates obtained corresponding to both roasting methods increased significantly with the roasting temperature but decreased slightly after the temperature reached 800 °C. In particular, the leaching rate of vanadium from CeO_2-promoted calcified roasting was consistently higher than that from calcified roasting at the same temperature. Combined with the TG-DSC curves in Figure 3, an exothermic peak occurs at 295 °C, and subsequently, the vanadium leaching rate is about 50% for both methods at this temperature. When the temperature increased from 600 to 750 °C, the vanadium leaching rate appeared to increase steeply, and the vanadium leaching rate for CeO_2-promoted calcined roasting reached 93.17% at 750 °C, which increased by 3.52% compared with that of calcined roasted vanadium at 750 °C, and was higher than that of calcined roasted vanadium at 800 °C. A slight decrease in the leaching rate was observed after 800 °C, which may be attributed to the sintering of the vanadium slag, resulting in an impediment to the leaching of vanadium.

The XRD pattern of vanadium slag produced by CeO_2-catalyzed calcification roasting at different temperatures is shown in Figure 5. At 295 °C, the physical phase was almost the same as that of the original slag. Combined with the TG-DSC curves in Figure 3, the weight loss and heat absorption peaks appeared before 295 °C, which were thought to be

https://doi.org/10.1021/acsomega.4c01211
ACS Omega 2024, 9, 16810−16819

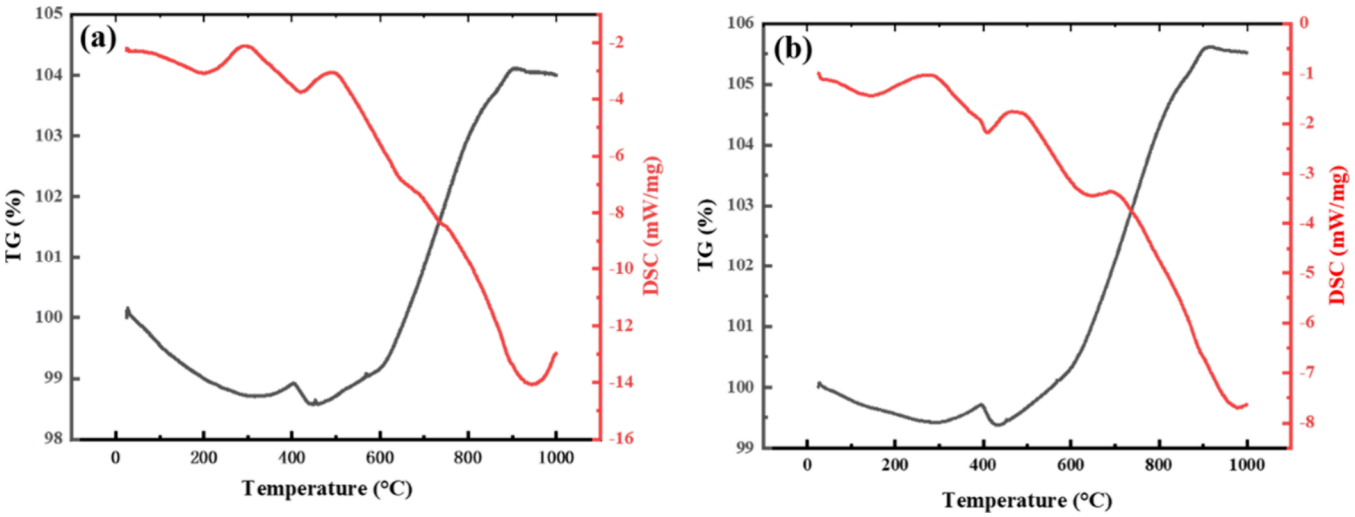

Figure 3. TG-DSC plots of (a) calcification and (b) CeO_2-catalyzed calcification of vanadium slag.

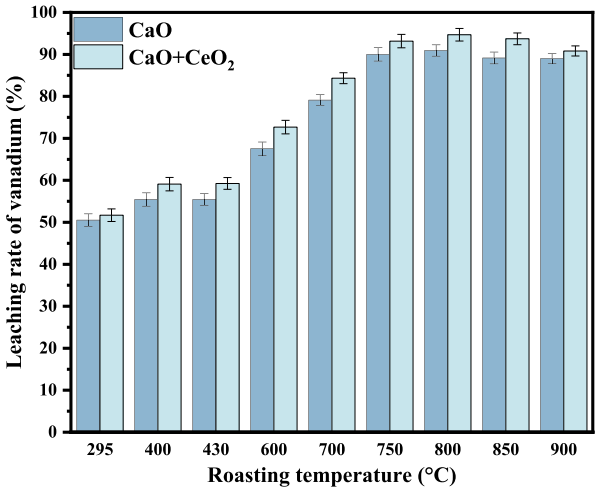

Figure 4. Effect of the roasting temperature on the leaching rate of vanadium.

caused by the dehydration of the free and internal bound water of the vanadium slag.

At 400 °C, $Fe_{2.95}Si_{0.05}O_4$ appeared in the physical phase, which was caused by the destruction of Fe_2SiO_4 in the olivine structure. The appearance of $Mg_{1.5}VO_4$ originates from the oxidation of vanadium−magnesium spinel MgV_2O_4, which is consistent with the apparent increase in thermogravimetry of the TG-DSC curve. At 430 °C, there was no obvious change in the physical phase, but a clear heat absorption peak and weight loss appeared on the TG-DSC curve, which may be due to the decomposition of $Mg(OH)_2$. At 600 °C, iron silicate was oxidized to form Fe_2O_3 and SiO_2, and SiO_2 thereafter combined with MnO to form $MnSiO_3$. Further oxidation of the spinel phase appears as $CrVO_3$, $Mg_2V_2O_7$, and V_2O_5.

After 600 °C, the TG-DSC curve shows that the weight of the sample increases sharply, and a clear exothermic peak appears, which is caused by the strong oxidation reaction of the spinel. At 700 °C, large amounts of calcium vanadate ($Ca_2V_2O_7$, $Ca_3V_2O_8$, $Ca_4V_2O_9$, and $Ca_5V_2O_{10}$) and manganese vanadate ($Mn_2V_2O_7$) appeared. At 750 °C, there is a new calcium vanadate phase, $Ca_2V_6O_{17}$. The formation of large amounts of vanadate leads to a substantial increase in the vanadium leaching rate. The phase changes at 800, 850, and

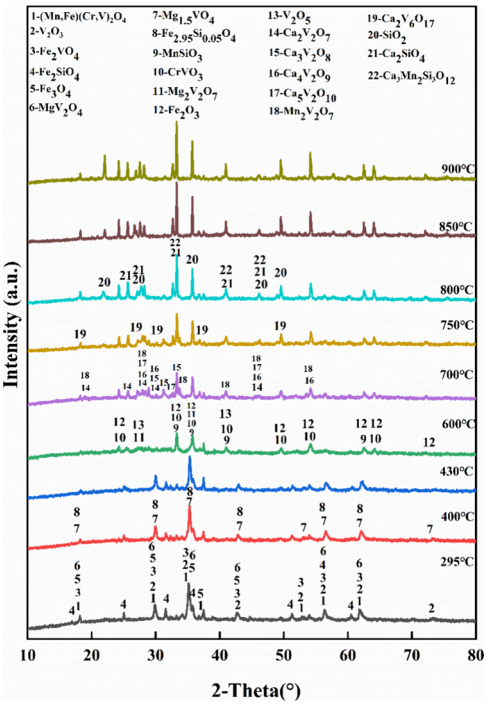

Figure 5. XRD patterns of clinker from CeO_2-catalyzed calcification roasting with different roasting temperatures.

900 °C were not obvious, and strong diffraction peaks of SiO_2, Ca_2SiO_4, and $Ca_3Mn_2Si_3O_{12}$ appeared.

SEM and EDS elemental mapping were used to study the changes in morphology and elemental distribution during the CeO_2-catalyzed calcification roasting process, focusing on the distribution of Ca, V, Fe, and Si elements, and the results are shown in Figure 6. Since a silicon wafer was used as a substrate for the SEM-EDS test, a large amount of Si was distributed around the sample. Analyzed in conjunction with XRD plots (Figures 1a and 5), in the raw slag, the distribution of Fe with V and Si elements is concentrated, indicating that it is mainly in the form of the olivine phase (Fe_2SiO_4) and the vanadium-bearing spinel phase. In particular, the absence of elemental V on the face of Si dispersion suggests that part of the olivine phase is encapsulated on the vanadium spinel, which increases

https://doi.org/10.1021/acsomega.4c01211
ACS Omega 2024, 9, 16810−16819

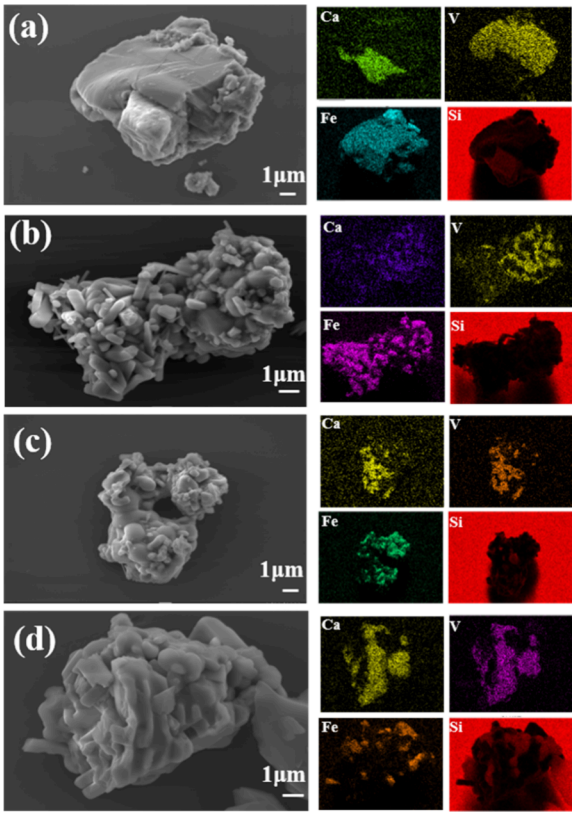

Figure 6. SEM-EDS plots of clinker by CeO_2-catalyzed calcification roasting at different temperatures: (a) raw slag; (b) 750 °C; (c) 800 °C; (d) 850 °C.

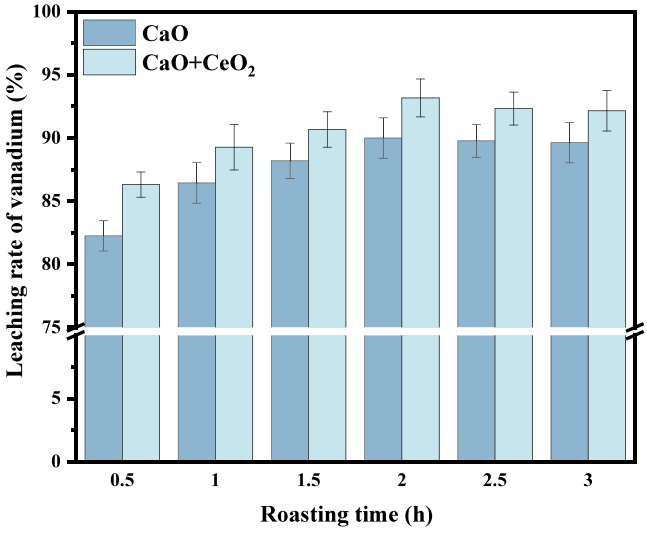

Figure 7. Effect of roasting time on vanadium leaching rate roasted at 750 °C.

the impediment to vanadium leaching and leads to a reduction in its leaching rate. At 750 °C, the Ca and V distributions are concentrated, which confirms the production of large amounts of calcium vanadate. Meanwhile, the absence of Si on the surface of the samples suggests that the olivine phase was damaged by the high temperatures, allowing more vanadium-bearing spinel to be revealed on the surface, leading to an increased vanadium leaching rate. At 800 °C, Ca and V are more concentrated, but Si appears on the surface of the

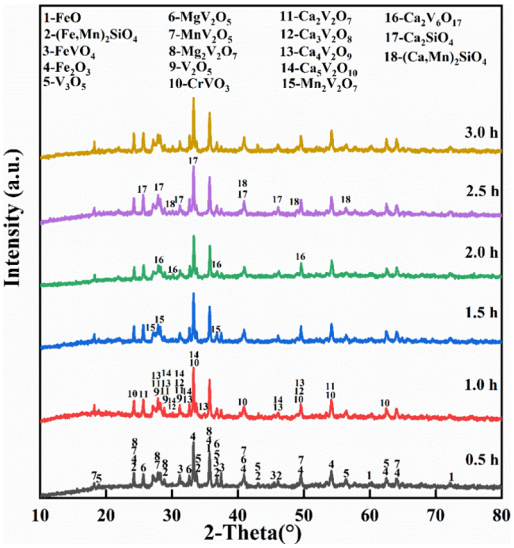

Figure 8. XRD patterns of clinker from CeO_2-catalyzed calcification roasting with different roasting times.

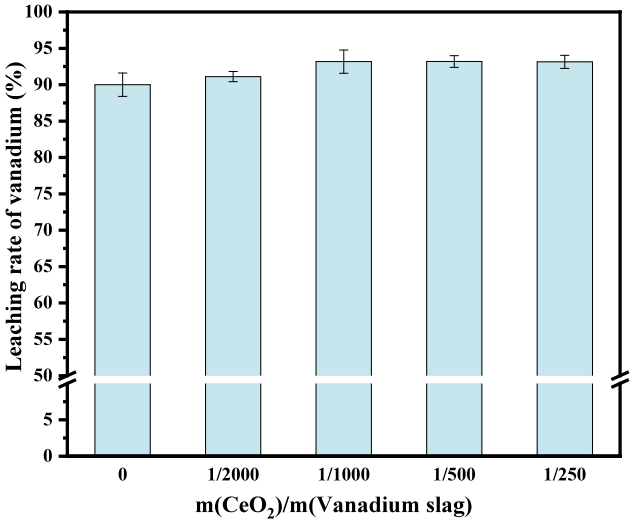

Figure 9. Effect of CeO_2 ratio on the vanadium leaching rate.

sample, which is a sign of sintering caused by melting at too high a temperature, which produces eutectic with a lower melting point of Si and encapsulates the vanadium slag. At 850 °C, the increase in Si on the samples suggests that sintering is more severe, which explains the slight decrease in vanadium leaching.

3.4. Effect of Roasting Time on Vanadium Slag.

Vanadium slag was mixed with a certain amount of CaO and CeO_2 ($n(CaO)/n(V_2O_5)$ = 1, $m(CeO_2)/m$(vanadium slag) = 1/1000); a control group was set up ($n(CaO)/n(V_2O_5)$ = 1) and roasted at 750 °C for different times; and the vanadium leaching rate was determined after leaching of the roasted material (leaching conditions: T = 80 °C, t = 30 min, 2 mol·L^{-1} sulfuric acid solution, liquid–solid ratio of 4:1 mL/g). The experimental results are shown in Figure 7.

The vanadium leaching rates from both roasting routes increased with the roasting time and finally showed stable values after 2 h of roasting. In particular, the vanadium leaching rate from the CeO_2-catalyzed calcified roasting was higher than that from calcified roasting for the same roasting time. When

https://doi.org/10.1021/acsomega.4c01211
ACS Omega 2024, 9, 16810−16819

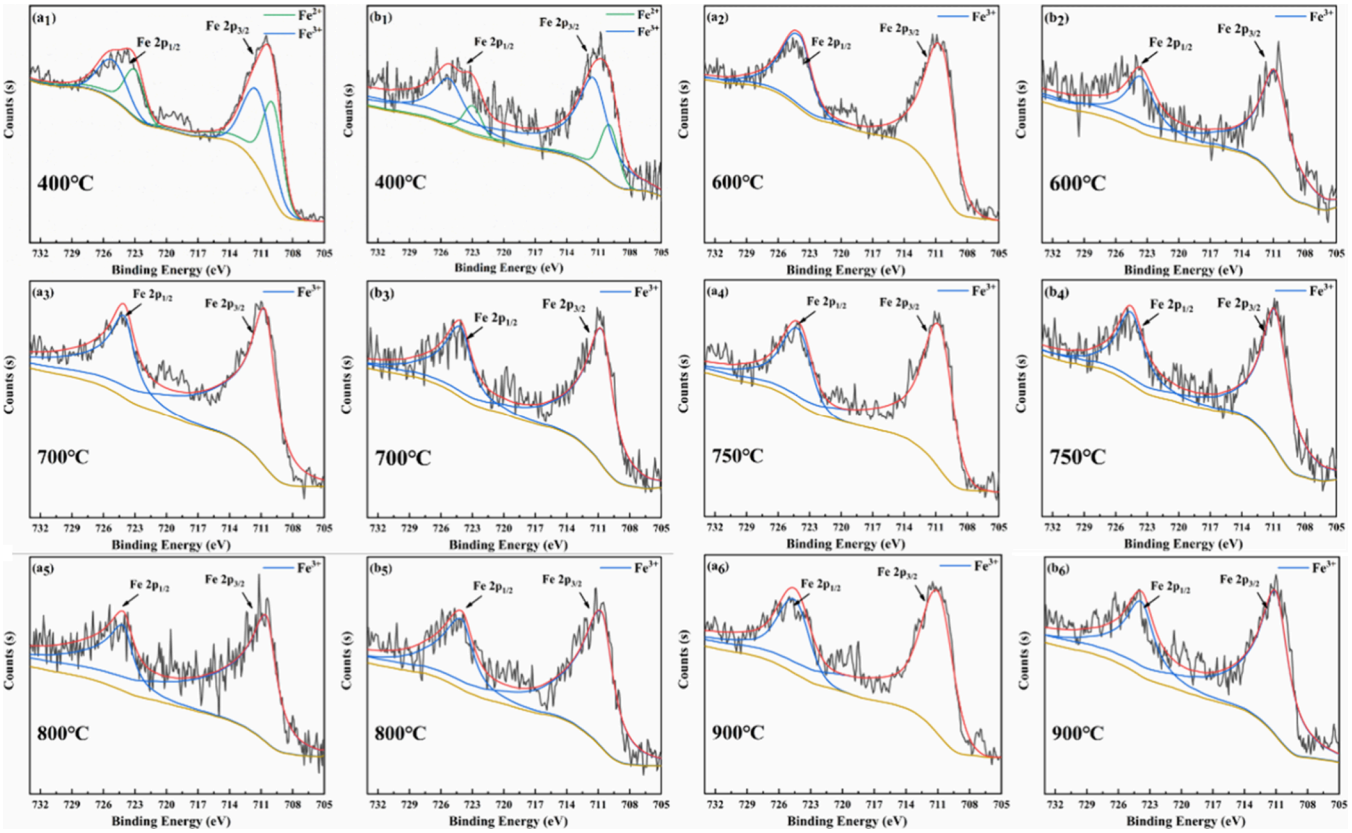

Figure 10. Fe 2p XPS profiles of vanadium slag after (a) CaO and (b) CaO-CeO_2 roasting

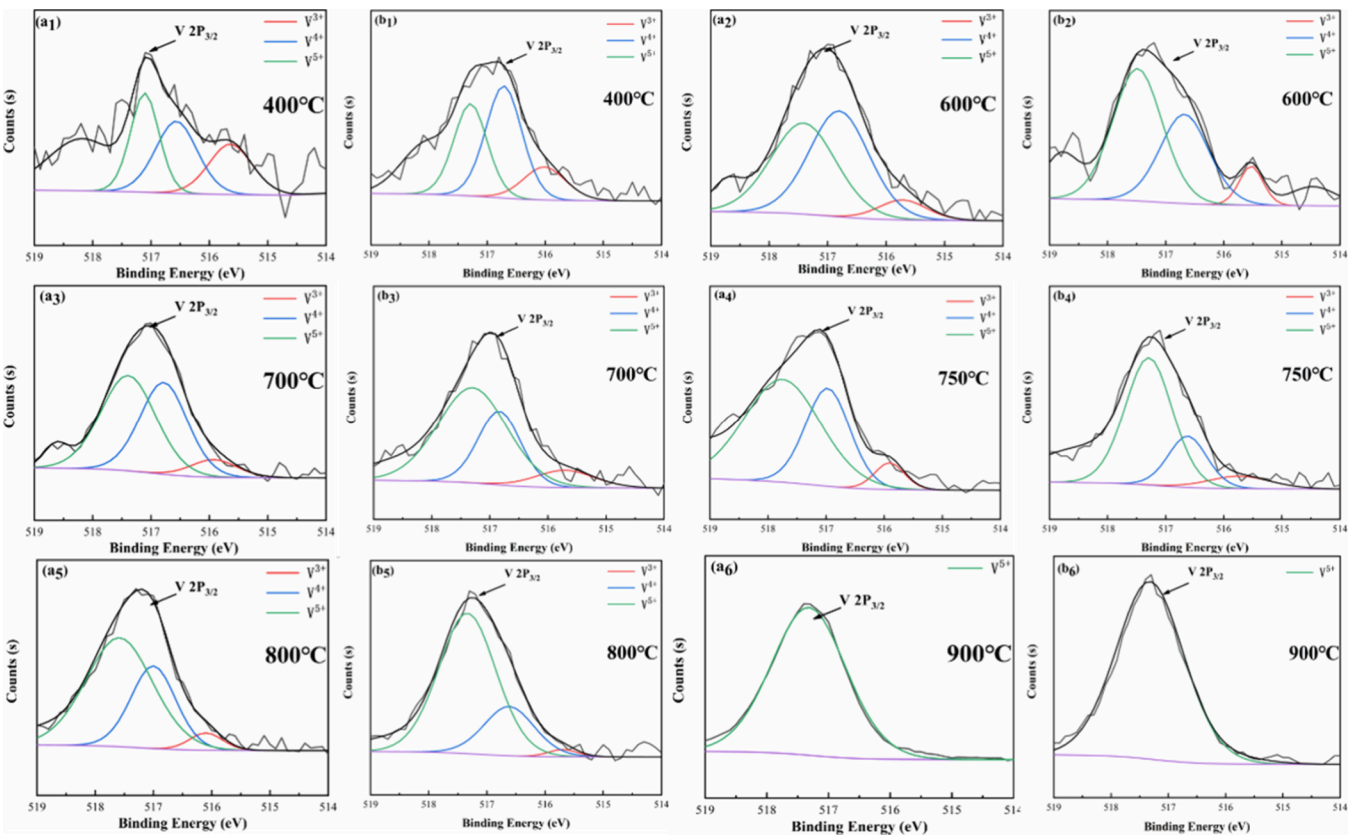

Figure 11. V $2p_{3/2}$ XPS profiles of vanadium slag after (a) CaO and (b) CaO-CeO_2 roasting.

https://doi.org/10.1021/acsomega.4c01211
ACS Omega 2024, 9, 16810−16819

Table 2. Content of V Element of Different Valences in Noncatalytic and CeO_2-Catalytic Roasting at Different Temperatures

method	temperature (°C)	V(III) (%)	V(IV) (%)	V(V) (%)
calcified roasting	400	27.20	37.50	35.30
	600	7.22	47.84	44.94
	700	7.75	41.90	50.35
	750	6.08	33.46	60.46
	800	4.94	32.03	63.03
	900	0.00	0.00	100.00
CeO_2-catalytic calcified roasting	400	16.36	47.59	36.05
	600	7.79	36.87	55.34
	700	9.42	29.18	61.40
	750	8.83	22.59	68.58
	800	1.96	23.18	74.86
	900	0.00	0.00	100.00

the roasting time was increased from 0.5 to 2.0 h, the vanadium leaching rate from CeO_2-catalyzed calcified roasting increased from 86.31 to 93.17% and increased by 3.52% compared to the vanadium leaching rate from calcified roasting at the same roasting time. When the roasting time exceeded 2.0 h, the vanadium leaching rate was observed to maintain almost stable, which indicated the optimized roasting time for both roasting routes.

Figure 8 shows the XRD pattern of CeO_2-catalyzed calcification roasting at 750 °C for different roasting times. After 0.5 h of roasting, the occurrence of Fe_2O_3 is due to the oxidation of FeO and Fe-olivine phases, and the occurrence of V_3O_5, MgV_2O_5, MnV_2O_5, and $Mg_2V_2O_7$ suggests that the vanadium spinel underwent decomposition and oxidation. After 1.0 h of roasting, the disappearance of the $(Fe, Mn)_2SiO_4$ peak indicates that the olivine phase is broken. $CrVO_3$ and a large number of calcium vanadate phases ($Ca_2V_2O_7$, $Ca_3V_2O_8$, $Ca_4V_2O_9$, and $Ca_5V_2O_{10}$) appeared with further oxidation of the vanadium spinel. An increase in the intensity of the diffraction peaks of the vanadate phase was observed with the increase in roasting time, and $Mn_2V_2O_7$ and $Ca_2V_6O_{17}$ appeared at 1.5 and 2.0 h, respectively, during which a large number of vanadate phases were generated leading to an increase in the vanadium leaching rate. After 2.5 h of roasting, Ca_2SiO_4 and $(Ca, Mn)_2SiO_4$ diffraction peaks appeared, which was attributed to the production of low-melting-point eutectic due to the prolonged roasting time, which wrapped around the surface of vanadium-containing phases and hindered the continued growth of vanadate.

3.5. Effect of CeO_2 Ratio on Vanadium Slag Roasting. Vanadium slag was mixed with a certain amount of CaO and different ratios of CeO_2 ($n(CaO)/n(V_2O_5)$ = 1), and the mixture was roasted at 750 °C for 2 h. The leaching rate of vanadium was determined after leaching the roasted material (leaching conditions: T = 80 °C, t = 30 min, 2 mol·L^{-1} sulfuric acid solution, liquid−solid ratio 4:1 mL/g). The experimental results are shown in Figure 9.

As the proportion of CeO_2 increased, vanadium leaching was the first to increase and then stabilized. Vanadium leaching increased with increasing CeO_2 until $m(CeO_2)/m$(vanadium slag) = 1/1000. This is because CeO_2 is stored in oxygen vacancies to form lattice oxygen when there is sufficient oxygen, which promotes the oxidation of the vanadium slag and converts the low-valent vanadium in the slag to the high-valent state, thus increasing the leaching rate. Further, the vanadium leaching rate is almost constant after $m(CeO_2)/m$(vanadium slag) = 1/1000, which may be due to the fact that vanadium on the surface of the slag has been completely leached.

3.6. Valence Variations of Vanadium Slag in CeO_2-Catalyzed Roasting. To further investigate the changes of elemental valence states in vanadium slag during the roasting process of vanadium slag, X-ray photoelectron spectroscopy (XPS) was used to characterize the calcified roasting clinker and CeO_2-catalyzed calcified roasting clinker at 400, 600, 700, 750, 800, and 900 °C, respectively (Figures 10 and 11, and Table 2). The valence states of the elements V and Fe in vanadium slag change significantly with the roasting temperature. As the roasting temperature increases, both elements are converted to higher valence states.

After calcareous roasting at 400 °C, the binding energies of $2p_{3/2}$ and $2p_{1/2}$ were 709.85 and 723.01 eV for Fe(II) and

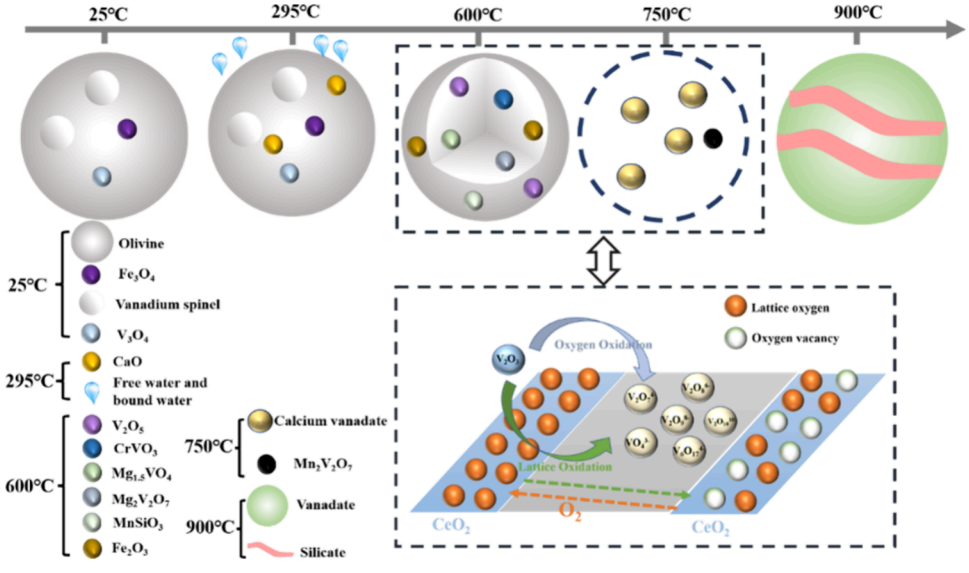

Figure 12. Schematic diagram of the vanadium slag catalytic calcification roasting reaction.

https://doi.org/10.1021/acsomega.4c01211
ACS Omega 2024, 9, 16810−16819

Table 3. Main Chemical Reactions in CeO_2-Catalyzed Calcified Vanadium Slag Roasting

temperature range	main reaction
RT ~ 295 °C	dehydration
295−600 °C	$2Fe_2SiO_4 + O_2 = 2Fe_2O_3 + 2SiO_2$
	$4Fe_3O_4 + O_2 = 6Fe_2O_3$
	$2MgV_2O_4 + O_2 = Mg_2V_2O_7 + V_2O_3$
	$3MgV_2O_4 + O_2 = 2Mg_{1.5}VO_4 + 2\ V_2O_3$
	$4FeV_2O_4 + O_2 = 2Fe_2O_3 + 4\ V_2O_3$
	$4MnV_2O_4 + O_2 = 2Mn_2O_3 + 4\ V_2O_3$
	$MnO + SiO_2 = MnSiO_3$
	$V_2O_3 + O_2 = V_2O_5$
	$4FeCr_2O_4 + O_2 + 4\ V_2O_3 = 2Fe_2O_3 + 8CrVO_3$
600−750 °C	$V_2O_5 + 2CaO = Ca_2V_2O_7$
	$V_2O_5 + 3CaO = Ca_3V_2O_8$
	$V_2O_5 + 4CaO = Ca_4V_2O_9$
	$V_2O_5 + 5CaO = Ca_5V_2O_{10}$
	$3\ V_2O_5 + 2CaO = Ca_2V_6O_{17}$
	$2\ V_2O_3 + 4CeO_2 + 4CaO + O_2 = 2Ca_2V_2O_7 + 2Ce_2O_3$
	$2\ V_2O_3 + 4CeO_2 + 6CaO + O_2 = 2Ca_3V_2O_8 + 2Ce_2O_3$
	$2\ V_2O_3 + 4CeO_2 + 8CaO + O_2 = 2Ca_4V_2O_9 + 2Ce_2O_3$
	$2\ V_2O_3 + 4CeO_2 + 10CaO + O_2 = 2Ca_5V_2O_{10} + 2Ce_2O_3$
	$6\ V_2O_3 + 4CeO_2 + 4CaO + 5O_2 = 2Ca_2V_6O_{17} + 2Ce_2O_3$
	$2Ce_2O_3+O_2 = 4CeO_2$
	$2\ V_2O_3 + 2Mn_2O_3+O_2 = 2Mn_2V_2O_7$
750−900 °C	$SiO_2 + 2CaO = Ca_2SiO_4$
	$3SiO_2 + 3CaO + Mn_2O_3 = Ca_3Mn_2Si_3O_{12}$

711.31 and 725.11 eV for Fe(III), respectively, and the proportion of Fe(III) to Fe element was 49.60%. While the vanadium slag was roasted by CeO_2-catalyzed calcification at 400 °C, the binding energies of $2p_{3/2}$ and $2p_{1/2}$ of Fe(II) were 710.17 and 722.97 eV, respectively; those of $2p_{3/2}$ and $2p_{1/2}$ of Fe(III) were 711.44 and 725.24 eV, respectively; and the percentage of Fe(III) was as high as 81.26%. It is shown that the rate of Fe(II) oxidation is increased in CeO_2-catalyzed calcification roasting. When the roasting temperature reached 600 °C, only peaks of Fe (III) were presented, which is consistent with the XRD results of the presence of only Fe_2O_3 at 600 °C.

The binding energies of $2p_{3/2}$ for V(III), V(IV), and V(V) in calcified roasting and CeO_2-catalyzed calcified roasting were 515.8 516.5, and 517.2 eV, respectively. Through the peak fitting and area integration of the V signals, the proportions of each valence state of V are calculated (Table 2). The pentavalent vanadium valence state increases with temperature for both methods, suggesting that an increase in temperature converts vanadium to the higher valence states of vanadium. More pentavalent vanadium was produced by CeO_2-catalyzed calcified roasting relative to calcified roasting at the same roasting temperature, suggesting that CeO_2-catalyzed calcified roasting results in a significant increase in the vanadium oxidation rate, which is consistent with the fact that the vanadium leaching rate of CeO_2-catalyzed calcified roasting is higher than that of calcified roasting (Figure 4). The proportion of pentavalent vanadium to total vanadium was 100% for both methods at the roasting temperature of 900 °C. However, the leach rate of vanadium decreases for those roasted at 900 °C, which was ascribed to the sintering of the silicon-containing salts covering the surface of the vanadate and inhibiting the leaching process.

3.7. Mechanism of CeO_2-Catalyzed Roasting. Based on the above experimental results, the main chemical reaction equations and schematic diagrams of compound changes in vanadium slag during catalytic calcification roasting were summarized, as shown in Figure 12 and Table 3. The free and intramolecularly bound water of the vanadium slag is removed at 25−295 °C. At 295−600 °C, the Fe-olivine phase is destroyed by high temperatures and oxidized to Fe_2O_3; the vanadium spinel phase is exposed on the surface over a large area; and a variety of vanadate phases are generated by catalytic oxidation. Various forms of calcium vanadate ($Ca_2V_2O_7$, $Ca_3V_2O_8$, $Ca_4V_2O_9$, $Ca_5V_2O_{10}$, and $Ca_2V_6O_{17}$) and $Mn_2V_2O_7$ appeared at 600−750 °C. This is the most violent stage of the oxidation reaction; during this process, molecular oxygen captures electrons from vanadium of low valence and results in the direct oxidization of the vanadium slag. After introducing CeO_2 in roasting slag, CeO_2 can play a catalytic role in the oxidation of vanadium slag by supplying active oxygen species and hereafter the activation of oxygen molecules. The cerium ions readily switch between the oxidation states of Ce^{3+} and Ce^{4+}, and the valence transition process may be accompanied by the formation and disappearance of oxygen vacancies, which allows cerium dioxide to release or adsorb oxygen under reducing or oxidizing conditions. At 750−900 °C, the vanadate phase is gradually encapsulated by the silicate phase.

4. CONCLUSIONS

In this paper, a new method of vanadium extraction from vanadium slag by catalytic calcification roasting acid leaching with low energy consumption, high efficiency, and cleanliness was proposed by introducing trace CeO_2 as a catalyst in the process of vanadium slag calcification roasting. CeO_2 plays a similar role to store−release O_2 during vanadium slag roasting, and the lattice oxygen in CeO_2 is replenished in time when the ambient O_2 atmosphere is insufficient to intensify the oxidation reaction with vanadium slag. Under the same

https://doi.org/10.1021/acsomega.4c01211
ACS Omega 2024, 9, 16810−16819

conditions, the vanadium leaching rate of the catalytic system was always higher than that of the noncatalytic system, and the ratio of V(V) to total V was always higher in the CeO_2 catalytic system than in the noncatalytic system in XPS. The results of XRD and SEM-EDS show that the catalytic system generates a large amount of vanadate when the roasting temperature is 600−750 °C, and a silicate phase adheres to the vanadate surface at temperatures higher than 800 °C, which affects the leaching of vanadium. The roasting−leaching experiments showed that under the optimum conditions of roasting temperature of 750 °C, roasting time of 2 h, CeO_2 of 0.1 wt %, leaching temperature of 80 °C, leaching time of 30 min, 2 $mol{\cdot}L^{-1}$ sulfuric acid solution, and liquid-to-solid ratio of 4:1 mL/g, the vanadium leaching rate reached 93.17%, which was higher than that of the noncatalytic system at 800 °C. Therefore, CeO_2-catalyzed calcification roasting provides an alternative route to reduce the energy consumption problems associated with the sintering phenomenon caused by high roasting temperatures in the production process.

AUTHOR INFORMATION

Corresponding Authors

Jun Du − *College of Chemistry and Chemical Engineering, Chongqing University, Chongqing 400044, China;* orcid.org/0000-0003-3629-7144; Email: dujune@cqu.edu.cn

Changyuan Tao − *College of Chemistry and Chemical Engineering, Chongqing University, Chongqing 400044, China;* orcid.org/0009-0007-1475-9164; Email: taocy@cqu.edu.cn

Authors

Zongyuan Xu − *College of Chemistry and Chemical Engineering, Chongqing University, Chongqing 400044, China*

Kang Tang − *College of Chemistry and Chemical Engineering, Chongqing University, Chongqing 400044, China*

Yan Chen − *Pangang Group Steel Vanadium and Titanium Co Ltd, Panzhihua, Sichuan 617067, China*

Qian Zhang − *College of Chemistry and Chemical Engineering, Chongqing University, Chongqing 400044, China;* orcid.org/0009-0004-4339-4115

Zuohua Liu − *College of Chemistry and Chemical Engineering, Chongqing University, Chongqing 400044, China;* orcid.org/0000-0003-4229-0168

Complete contact information is available at: https://pubs.acs.org/10.1021/acsomega.4c01211

Author Contributions

[§]Z.X. and K.T. contributed equally.

Notes

The authors declare no competing financial interest.

ACKNOWLEDGMENTS

This work was supported by the Science and Technology Project of Panzhihua Iron and Steel Research Institute Limited Company [grant number YYFJS2021001].

REFERENCES

(1) Moskalyk, R. R.; Alfantazi, A. M. Processing of vanadium: a review. *Minerals Engineering* **2003**, *16* (9), 793−805. Hui, X.; Zhang, J.; Liang, Y.; Chang, Y.; Zhang, W.; Zhang, G. Comparison and evaluation of vanadium extraction from the calcification roasted vanadium slag with carbonation leaching and sulfuric acid leaching. *Sep. Purif. Technol.* **2022**, *297*, No. 121466. Wang, W.; Wang, W.; Sun, Q. Utilization of Vanadium Slag and Iron-Rich Red Mud for the Fabrication of Fe−V Alloy: Mechanism and Performance Analysis. *Journal of Sustainable Metallurgy* **2023**, *9* (1), 341−349.

(2) Guo, K.; Xiang, J.; Zhang, N.; Huang, Q.; Li, L.; Lv, X. Effect of mechanical activation on the extraction of vanadium from vanadium slag pellet by sodium roasting followed by water leaching process. *Canadian Metall. Q.* **2024**, *63*, 186−193. Teng, Q.; Yang, Z.-C.; Wang, H.-J. Recovery of vanadium and nickel from spent-residue oil hydrotreating catalyst by direct acid leaching-solvent extraction. *Transactions of Nonferrous Metals Society of China* **2023**, *33* (1), 325−336. Gao, F.; Olayiwola, A. U.; Liu, B.; Wang, S.; Du, H.; Li, J.; Wang, X.; Chen, D.; Zhang, Y. Review of Vanadium Production Part I: Primary Resources. *Mineral Processing and Extractive Metallurgy Review* **2022**, *43* (4), 466−488. Li, H.-Y.; Cheng, J.; Wang, C.-J.; Shen, S.; Diao, J.; Xie, B. Ecofriendly Selective Extraction of Vanadium from Vanadium Slag with High Chromium Content via Magnesiation Roasting−Acid Leaching. *Metallurgical and Materials Transactions B* **2022**, *53* (1), 604−616.

(3) Peng, H.; Guo, J.; Li, B.; Huang, H. Vanadium properties, toxicity, mineral sources and extraction methods: a review. *Environmental Chemistry Letters* **2022**, *20* (2), 1249−1263.

(4) Langeslay, R. R.; Kaphan, D. M.; Marshall, C. L.; Stair, P. C.; Sattelberger, A. P.; Delferro, M. Catalytic Applications of Vanadium: A Mechanistic Perspective. *Chem. Rev.* **2019**, *119* (4), 2128−2191. An, Y.; Ma, B.; Li, X.; Chen, Y.; Wang, C.; Wang, B.; Gao, M.; Feng, G. A review on the roasting-assisted leaching and recovery of V from vanadium slag. *Process Safety Environ. Protect.* **2023**, *173*, 263−276.

(5) Liu, L.; Kauppinen, T.; Tynjälä, P.; Hu, T.; Lassi, U. Water leaching of roasted vanadium slag: Desiliconization and precipitation of ammonium vanadate from vanadium solution. *Hydrometallurgy* **2023**, *215*, No. 105989.

(6) Cheng, J.; Li, H. Y.; Hai, D.; Chen, X. M.; Diao, J.; Xie, B. Magnesiation roasting kinetics exploration of vanadium slag toward minimization of tailing toxicity. *J. Hazard Mater.* **2023**, *452*, No. 131378.

(7) Wang, Z.; Chen, L.; Aldahrib, T.; Li, C.; Liu, W.; Zhang, G.; Yang, Y.; Luo, D. Direct recovery of low valence vanadium from vanadium slag — Effect of roasting on vanadium leaching. *Hydrometallurgy* **2020**, *191*, No. 105156.

(8) Kang, Q.; Zhang, Y.; Bao, S. An environmentally friendly hydrothermal method of vanadium precipitation with the application of oxalic acid. *Hydrometallurgy* **2019**, *185*, 125−132.

(9) Xiang, J.-Y.; Wang, X.; Pei, G.-S.; Huang, Q.-Y.; LÜ, X.-W. Recovery of vanadium from vanadium slag by composite roasting with CaO/MgO and leaching. *Transactions of Nonferrous Metals Society of China* **2020**, *30* (11), 3114−3123.

(10) Deng, R.; Xie, Z.; Liu, Z.; Tao, C. Leaching kinetics of vanadium catalyzed by electric field coupling with sodium persulfate. *J. Electroanal. Chem.* **2019**, *854*, No. 113542. Diao, J.; Liu, L.; Lei, J.; Tan, W.-F.; Li, H.-Y.; Xie, B. Oxidation Mechanism of Vanadium Slag with High MgO Content at High Temperature. *Metallurgical and Materials Transactions B* **2021**, *52* (1), 494−501. Yu, T.; Jiang, T.; Wen, J.; Sun, H.; Li, M.; Peng, Y. Effect of chemical composition on the element distribution, phase composition and calcification roasting process of vanadium slag. *International Journal of Minerals, Metallurgy and Materials* **2022**, *29* (12), 2144−2151.

(11) Deng, R.; Xie, Z.; Liu, Z.; Deng, L.; Tao, C. Enhancement of vanadium extraction at low temperature sodium roasting by electric field and sodium persulfate. *Hydrometallurgy* **2019**, *189*, No. 105110.

(12) Dong, Z.; Zhang, J.; Yan, B. A New Approach for the Comprehensive Utilization of Vanadium Slag. *Metallurgical and Materials Transactions B* **2022**, *53* (4), 2198−2208. Wang, Z.; Chen, L.; Qin, Z.; Yang, K.; Liang, B.; Zhang, G.; Liu, C.; Luo, D. A green and efficient route for simultaneous recovery of low valence of vanadium and chromium, titanium and iron from vanadium slag. *Resour., Conserv. Recycl.* **2022**, *178*, No. 106046. Wen, J.; Yu, T.; Jiang, T.; Sun, H.; Li, M.; Peng, Y. Effect of chromium content on the phase

composition, crystallization and components extraction of vanadium slag. *Process Safety and Environmental Protection* **2022**, *165*, 13−21. Wen, J.; Jiang, T.; Yu, T.; Chen, B.; Li, L. Clean and efficient extraction of vanadium from vanadium slag: Effect of manganese on the phase composition and vanadium extraction process. *J. Cleaner Prod.* **2022**, *367*, No. 133077.

(13) Cai, Z.; Zhang, Y.; Liu, T.; Huang, J. Mechanisms of Vanadium Recovery from Stone Coal by Novel $BaCO_3$/CaO Composite Additive Roasting and Acid Leaching Technology. *Minerals* **2016**, *6* (2), 26.

(14) Wen, J.; Jiang, T.; Sun, H.; Yu, T. Novel Understanding of Simultaneous Extraction of Vanadium and Manganese from Vanadium Slag and Low-Grade Pyrolusite Based on Selective Oxidation−Reduction Roasting. *ACS Sustainable Chem. Eng.* **2020**, *8* (15), 5927−5936.

(15) Gao, H.; Jiang, T.; Zhou, M.; Wen, J.; Li, X.; Wang, Y.; Xue, X. Effect of microwave irradiation and conventional calcification roasting with calcium hydroxide on the extraction of vanadium and chromium from high-chromium vanadium slag. *Min. Eng.* **2020**, *145*, No. 106056.

(16) Song, Z.; Wei, Y.; Ma, Z. A.; Zhang, X.; Mao, Y.; Luo, J.; Zhu, X.; Liu, W.; Jin, J. Influence of different sources of cerium on the oxidation-reduction ability and oxygen vacancies of CeO_2-MnO in the catalytic oxidation of toluene. *Surf. Interfaces* **2021**, *24*, No. 101042.

(17) Li, Y.; Li, H.; Li, K.; Wang, R.; Zhang, R.; Liu, R. Roles of Oxygen Vacancies in CeO_2 Nanostructures for Catalytic Aerobic Cyclohexane Oxidation. *ACS Applied Nano Materials* **2023**, *6* (15), 14214−14227.

(18) Montini, T.; Melchionna, M.; Monai, M.; Fornasiero, P. Fundamentals and Catalytic Applications of CeO_2-Based Materials. *Chem. Rev.* **2016**, *116* (10), 5987−6041. Chen, J.; Pham, H. N.; Mon, T.; Toops, T. J.; Datye, A. K.; Li, Z.; Kyriakidou, E. A. Ni/CeO_2 Nanocatalysts with Optimized CeO_2 Support Morphologies for CH_4 Oxidation. *ACS Applied Nano Materials* **2023**, *6* (6), 4544−4553. Matussin, S. N.; Khan, F.; Harunsani, M. H.; Kim, Y.-M.; Khan, M. M. Effect of Pd-Doping Concentrations on the Photocatalytic, Photoelectrochemical, and Photoantibacterial Properties of CeO_2. *Catalysts* **2023**, *13* (1), 96. Zedan, A. F.; Moussa, S.; El-Shall, M. S. Rational synthesis of gold-ceria catalysts supported on reduced graphene oxide with remarkable activity for CO oxidation. *Mater. Res. Express* **2023**, *10*, No. 025007.

(19) Utara, S.; Jantachum, P.; Hunpratub, S.; Chanlek, N.; Phokha, S. Enhanced dielectric constant and mechanical investigation of epoxidized natural rubber with TM-doped CeO_2 nanocomposites. *J. Alloys Compd.* **2023**, *939*, No. 168601.

https://doi.org/10.1021/acsomega.4c01211
ACS Omega 2024, 9, 16810−16819